STM Study of Terephthalic Acid Self-Assembly on Au(111): Hydrogen-Bonded Sheets on an Inhomogeneous Substrate†

Sylvain Clair,*,‡ Stéphane Pons,‡ Ari P. Seitsonen,§ Harald Brune,‡ Klaus Kern,‡,|| and Johannes V. Barth*,‡,⊥

Institut de Physique des Nanostructures (IPN), Ecole Polytechnique Fédérale de Lausanne, CH-1015 Lausanne, Switzerland, Physikalisch Chemisches Institut (PCI), Universität Zürich, CH-8057 Zürich, Max-Planck-Institut für Festkörperforschung, D-70569 Stuttgart, Germany, and Advanced Materials and Process Engineering Laboratory, University of British Columbia, Vancouver, BC V6T 1Z4, Canada

Received: February 4, 2004; In Final Form: May 22, 2004

The adsorption and ordering of the molecule terephthalic acid (TPA), 1,4-benzene-dicarboxylic acid $C_6H_4(COOH)_2$, on the reconstructed Au(111) surface has been studied in situ in ultrahigh vacuum by scanning tunneling microscopy (STM) at room temperature. Two-dimensional (2D) self-assembled supramolecular domains evolve, wherein the well-known one-dimensional (1D) carboxyl H-bond pairing scheme is identified. Since the individual molecules occupy a distinct adsorption site and the supramolecular ordering usually extends over several substrate reconstruction domains, a significant variation in hydrogen bond lengths is encountered, which illustrates the versatility of hydrogen bridges in molecular engineering at surfaces. Ab initio calculations for a 1D H-bonded molecular chain provide insight into the limited geometric response of the molecules in different local environments.

Introduction

The deliberate construction of complex nanoscale assemblies using molecular building blocks is paramount for the development of novel functional materials. Particularly appealing is the engineering of supramolecular architectures, which are stabilized by noncovalent links such as hydrogen bonds or metal−ligand interactions.[1,2] Recent studies, where as an experimental technique predominantly scanning tunneling microscopy (STM) was employed, revealed that at well-defined surfaces nanoscale insight into molecular architecture and underlying self-assembly phenomena can be gained.[3−12] To develop a rationale for molecular engineering in two dimensions, we need a comprehensive understanding of the coupling schemes of adsorbed complex molecules mediated by their functional groups, their bonding to the employed solid substrates, and the organization principles resulting from the balance of these interactions. This understanding will pave the way toward novel bottom-up strategies for the fabrication of supramolecular nanostructures potentially useful as novel materials in molecular electronics, nanotemplating, chemical sensing schemes, host-guest interactions or catalysis.

A great variety of molecular building blocks comprising functional groups for hydrogen bond formation have been successfully exploited for the fabrication of highly organized assemblies in three dimensions.[13,14] Such species have been employed at surfaces to construct distinct low-dimensional architectures including clusters, chains, and nanoporous layers.[3−5,7,9,12,15,16] Here we report STM investigations addressing the bonding and supramolecular self-assembly of the molecule 1,4-benzenedicarboxylic acid (terephthalic acid, TPA; see Figure 1) on the reconstructed Au(111) surface at ambient temperature under ultrahigh-vacuum (UHV) conditions. TPA belongs to the family of aromatic molecules with exodentate carboxyl functionalities, which are frequently employed in three-dimensional (3D) crystal engineering[17,18] and have proven to be appropriate for supramolecular architecture at surfaces.[6,7,10,16,19,20] In the TPA bulk structure, the H-bonded chains typical of linear dicarboxylic acids are found.[21,22] It is of interest to find out whether this coupling scheme can be maintained in surface-supported arrangements. As a substrate, we have chosen the close-packed Au(111) surface, which provides small atomic corrugation and low chemical reactivity. Thus, the carboxylic acid groups are expected to be preserved at ambient temperature[23] (in contrast to carboxylate formation encountered on the more reactive Cu surfaces[6−8]). Moreover, the Au(111) chevron reconstruction[24] accounts for a substrate with natural dislocations patterns and varying interatomic spacing, which allows for an investigation of the response of hydrogen-bonded systems to such features.[15,25]

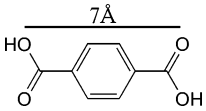

Figure 1. Molecular structure of terephthalic acid (TPA).

Experimental Section

All experiments were performed with a homebuilt[26] ultrahigh vacuum scanning tunneling microscope (UHV−STM) at room temperature. The system base pressure is 1×10^{-10}mbar. The Au(111) surface was prepared by repeated cycles of argon

† Part of the special issue "Gerhard Ertl Festschrift".

* To whom correspondence should be addressed. (S.C.) E-mail: sylvain.clair@epfl.ch. (J.V.B.) E-mail: johannes.barth@epfl.ch.

‡ Ecole Polytechnique Fédérale de Lausanne.

§ Universität Zürich.

|| Max-Planck-Institut für Festkörperforschung.

⊥ University of British Columbia.

10.1021/jp049501n CCC: $27.50
Published on Web 08/13/2004

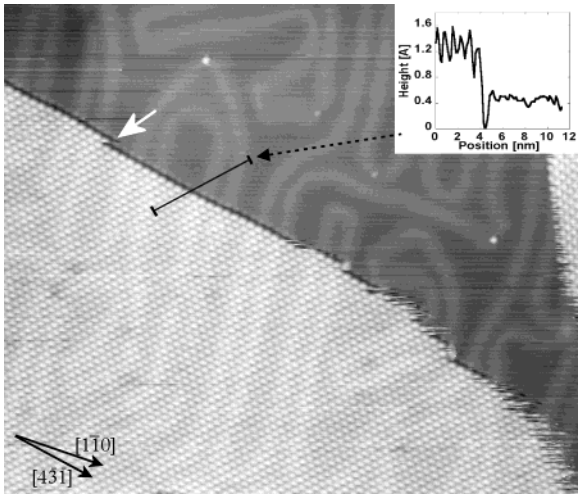

Figure 2. Typical organization of a hydrogen-bonded TPA layer on Au(111). The surface reconstruction is clearly visible on the entire imaged area. The inset shows a contour line along the indicated bar. The white arrow points to a site appearing as a kink (see discussion in the text). (STM image size 58 × 50 nm^2, $I = 0.4$ nA, $V = -470$ mV, TPA coverage 0.8 ML).

sputtering (900 V, 5 μA/cm^2) followed by annealing at 900 K. The TPA molecules (Fluka, >99%) were first outgassed in vacuum for several hours and then evaporated from a Knudsen cell at 150 °C onto the substrate kept at room temperature. This provides a deposition rate of about one monolayer (ML) per minute (one monolayer corresponds to a complete layer of the dense molecular phase). The STM head is of the Besocke type and runs with a commercial control electronics (RHK − SPM100). The STM tip is made out of an etched W wire (Ø 0.7 mm) and was Ar-bombarded in UHV. All data were acquired at room temperature in constant current mode, with typical tunneling resistances in the range of 10−1000 MΩ. In the figure captions V refers to the bias applied to the sample.

Results and Discussion

Samples with a coverage of one monolayer or less were prepared. At small concentrations, it is difficult to determine the exact coverage by STM at room temperature because the molecules are very mobile on the gold surface and form a two-dimensional molecular gas-phase where the molecules cannot be imaged individually. Upon increasing the density beyond about 0.5 ML the molecules condense into large compact well ordered domains. However these domains can be easily perturbed by lowering the tunnel resistance (approximately under 10 MΩ). Figure 2 shows the typical organization of the molecular layer. The chevron reconstruction of the Au(111) surface[24] is clearly visible in the upper part, where very mobile molecules are present, as well as underneath the TPA layer. The maintenance of the reconstruction indicates a weak coupling of the molecules to the substrate. The layer imaging height is 0.8 ± 0.1 Å above the surface covered by the 2D-gas phase, the intralayer molecular corrugation is 0.4 ± 0.1 Å. At the domain edge typically a gap of 0.2 ± 0.1 Å in depth occurs. The domain looks blurred on some parts of its border due to molecules that moved during the scan. We cannot discern whether this motion is diffusion along the boundary or an exchange with the 2D-gas phase by evaporation and recondensation. Kinks such as the one indicated by the white arrow in Figure 2 are rare, and domains are usually terminated by a complete row of molecules. We believe that this feature is not a real kink, rather presumably a complete row having evaporated into the 2D-gas phase when the tip was at this position. The domain edge here, along the [4$\bar{3}$1] direction, is much better defined than that in the lower right-hand part of the island, where the border appears frizzled. The higher stability of the [4$\bar{3}$1] edge direction reflects the anisotropic longitudinal/lateral intermolecular interactions. The individual TPA's are imaged as flat rodlike protrusions (about 7 Å × 5 Å) with dimensions fitting well with the size of a flat lying molecule. The observation of a preferred direction both on an individual molecular basis and arising from the domain stability determines the orientation of the molecules relative to each other (see inset Figure 3a), which is governed by the carboxylic acid dimerization via hydrogen bonding, as expected from the shape and functionality of the molecule (Figure 1). The formation of 2D molecular sheets furthermore suggests a lateral coupling between the 1D TPA chains, which is presumably mediated by weak hydrogen bonds or electrostatic interactions. The observed structure is similar to the one of TPA bulk and in agreement with investigations of related systems.[7,12,16,20] Apart from the reconstruction pattern of the underlying gold substrate, no long-range corrugation (indicative of a Moiré or a dislocation pattern) of the TPA sheets could be seen. Therefore, we deduce that the molecular layer is commensurate with the substrate and that the individual TPA's reside at a distinct adsorption site. The actual adsorption site could not be identified on the basis of the present experiments.

The TPA molecules arrange in a quasi-hexagonal lattice with different orientations relative to the substrate. Figure 3a shows four coexisting rotational domains. The rectangular shape delimiting a region covered by the 2D-gas phase is at first glance unexpected on a surface with hexagonal symmetry but can be easily explained by the molecular superstructure. We observed in total six equivalent orientational domains. Figure 3b shows the proposed model for the unit cell. For simplicity, we first consider the Au(111) surface plane as perfectly hexagonal (as the surface is reconstructed this is not exactly true; this point will be discussed below). Since the molecular lattice is not hexagonal, three rotational domains exist reflecting the substrate symmetry. In addition, within each rotational domain two chiral arrangements related by a mirror symmetry exist. The molecule itself is not chiral, neither in the gas phase nor in the adsorbed geometry. The specific adsorption site within the molecular lattice is neither chiral. The chiral symmetry break is induced exclusively from the oblique shape of the unit cell of the supramolecular 2D assembly representing an enantiomorphous entity.

The Fourier transforms of several images provide mean values for the unit cell parameter which are 8.3 ± 0.3 Å (along [0$\bar{1}$1]) and 10.0 ± 0.3 Å with an angle of 45° ± 3°. The quasi right angle between the domains seen in Figure 3a thus results from two adjacent mirror domains leading to an overall rotation of the molecular chains by 2 × 45°. We propose the following matrixes to describe the commensurate superstructure:

$$\begin{pmatrix} 3 & 0 \\ 1 & 3 \end{pmatrix}$$

and its mirror symmetry

$$\begin{pmatrix} 3 & -3 \\ -2 & -1 \end{pmatrix}$$

Note that this superstructure is referred to an ideal (111) plane; the exact superstructure matrix should also include the (22 × $\sqrt{3}$) gold reconstruction.

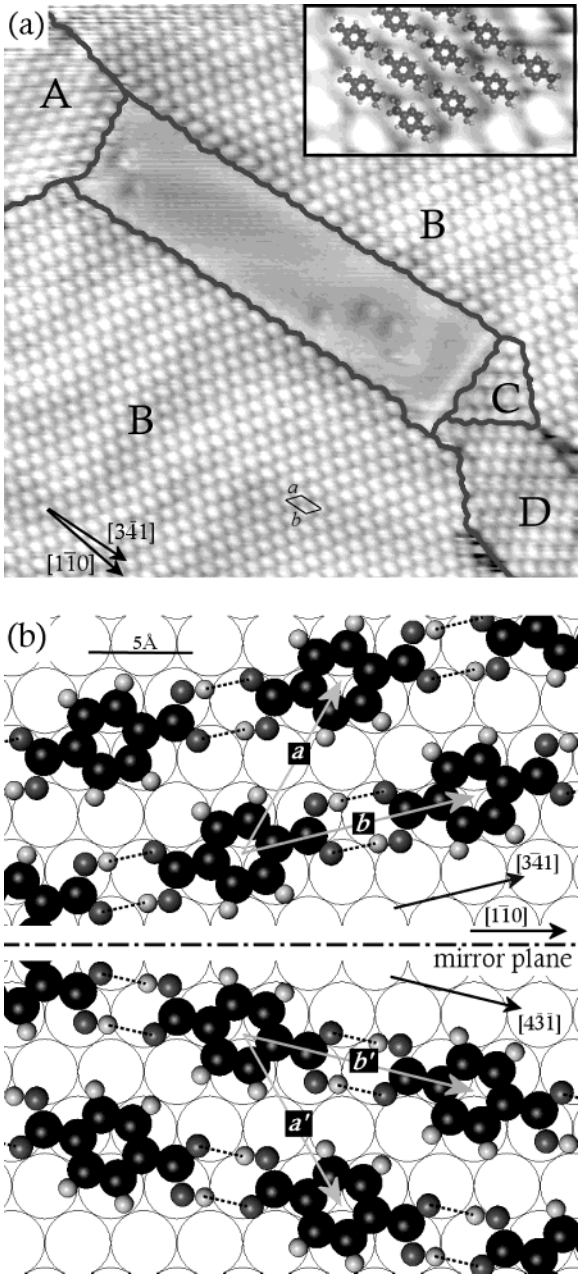

Figure 3. (a) Coexistence of different TPA rotational domains on Au(111). Four orientations are present: A, C, and D are rotated by 120° relative to each other; B represents the mirror symmetric arrangement of D with respect to [1$\bar{1}$0]. B is similarly the chiral counterpart to the domain in Figure 2 (STM image size 28 × 28 nm^2, $I = 0.5$ nA, $V = -20$ mV). The oval shape of the molecules and the anisotropy of the domain boundaries determine the molecular orientation (inset). (b) Model for the molecular superstructure; **a** (along the [0$\bar{1}$1] direction) and **b** (along the [3$\bar{4}$1] direction) are the lattice vectors, **a′** and **b′** are the base vectors for the lattice of opposite chirality (mirror symmetry of **a** and **b** with respect to [1$\bar{1}$0]). The hydrogen bonds are indicated by dashed lines. For simplicity the Au(111) substrate is modeled here as perfectly hexagonal. The molecule adsorption site is arbitrary.

The actually reconstructed Au(111) surface is not perfectly hexagonal, rather it is locally contracted in a ⟨1$\bar{1}$0⟩ direction.[24] The contraction direction does not extend over long distances, and a mesoscopic chevron arrangement with an alternating sequence of two rotational domains occurs at large terraces.[24,27,28] As the intermolecular distance is much smaller than the extension of these domains the molecular superstructure should be influenced by the distorted surface (analogous to simple superlattices on reconstructed Au(111), see ref 29).

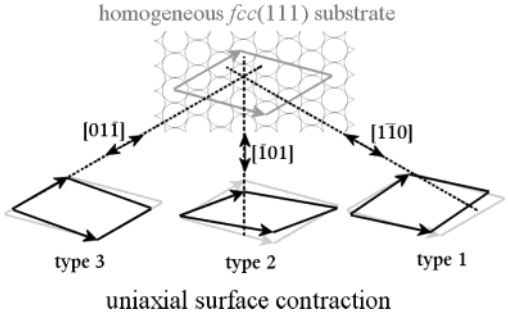

Figure 4. The effect of the Au(111) substrate reconstruction on the molecular lattice, and the dependence on the contraction direction. In gray is shown the molecular cell corresponding to a perfectly hexagonal substrate, in black the molecular cell uniaxially contracted along the direction indicated by the double arrow. The type numbers refer to Table 1.

TABLE 1: Dimensions of the Molecular Unit Cell which Depend on Its Orientation Relative to the Substrate Reconstruction[a]

type	reconstr.	*a* [Å]	*b* [Å]	γ	H-bond [Å]
1	[1$\bar{1}$0]	8.5 ± 0.1	9.9 ± 0.3	46.5°	2.9 ± 0.3
2	[$\bar{1}$01]	8.5 ± 0.1	10.3 ± 0.1	44.4°	3.3 ± 0.1
3	[01$\bar{1}$]	8.2 ± 0.3	10.1 ± 0.2	47.3°	3.1 ± 0.2
bulk					2.6[21]
TPA					2.7[22]

[a] As a consequence variations of the respective model-derived H-bond distances are encountered; the error margin comes from the local modulation of the contracted interatomic distance around its mean value. *a* is parallel to the [01$\bar{1}$] direction (see Figures 3 and 6). The reconstruction indicates the contraction direction. For comparison, values from bulk crystal are indicated.

The reconstruction corrugation typically amounts up to 0.2 Å over a distance of $^{44}/_{2}$ Å, which gives an out-of-plane correction of about 0.5°. The *fcc* to *hcp* site modulation produces a curvature in the lateral atomic alignment of the order of 0.8 Å over a distance of $^{63}/_{2}$ Å, which gives an in-plane correction of about 1.5°. These two effects give a correction for the intermolecular distance of the order of $a(1 - \cos\alpha) \approx 0.5$ pm and are neglected.

Therefore, we model the reconstructed surface as a uniaxially and homogeneously contracted hexagonal plane. In the contraction direction, we take a constant interatomic distance of 2.75 Å (the bulk interatomic distance is 2.88 Å). Note that in reality this distance oscillates around this value with an amplitude of ±0.1 Å over the period of the reconstruction (23 surface atomic spacings). In the two other close-packed directions, the interatomic distance is assumed to be 2.85 Å.

The distortion of the reconstructed surface is transmitted into the molecular lattice, as shown schematically in Figure 4. Depending on its orientation relative to the surface contraction direction, we find three different unit cells, labeled type 1, 2, and 3, whose parameters are indicated in Table 1. Although these differences are close to the experimental error, we could find direct evidence. Figure 5 shows a single molecular domain extending over two gold reconstruction domains. The upper region of the domain is of type 1 while the lower region is of type 2. As shown in the Fourier transform of the two regions, the respective lattice parameters have distinct differences. To explain these differences in more details, the molecular domain are modeled in Figure 6. The contraction direction, varying from [1$\bar{1}$0] to [$\bar{1}$01] influences directly the intermolecular distances (and the hydrogen bond lengths) and induces also small differences in the lattice orientation.

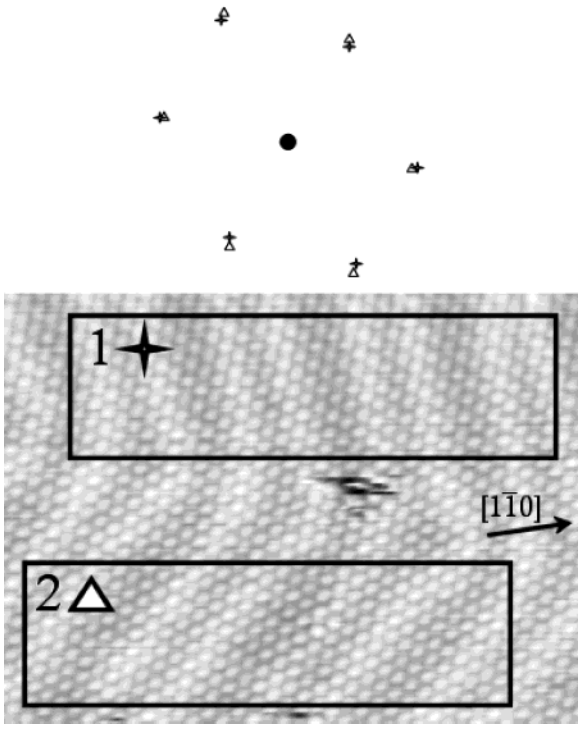

Figure 5. Lower part: STM image of a single molecular domain extending over two substrate reconstruction domains (image size 35 $\times$ 22 nm^2, $I = 0.4$ nA, $V = -400$ mV). Upper part: Fourier transform of the two regions marked 1 and 2, corresponding to the two orientations of the reconstruction detailed in Table 1 and modeled in Figure 6. While the intermolecular coupling scheme is maintained in the entire molecular layer, it adapts locally to the reconstructed gold lattice so that slightly different unit cell parameters are found in the two regions. Note that the Fourier image refers to the center of the spots which are in reality smeared because, apart from the experimental error, the local variations of the contracted interatomic distance around its mean value induces local variations of the intermolecular distances up to a few %.

We never obtained sufficiently high resolution in the STM images to resolve the individual functional groups of the molecule. This is generally the case in UHV studies, in agreement with the current theoretical understanding in STM imaging of organic molecules.[30] The situation is different for images acquired in solution as in ref 20 where various and not well understood effects may interfere. The resolution obtained in this case is still subjected to discussion.[31] Nevertheless, it is possible for our system to characterize the hydrogen bond lengths between the molecules by analyzing the modeled superstructure. The three unit cells of Table 1 give three different values for the distance between the oxygen atoms in the hydrogen bond. These are respectively 2.9, 3.3, and 3.1 Å. Although the contraction of the reconstructed substrate amounts locally to 4−6%, the differences in the hydrogen bond reaches up to 20% since a molecule extends over several gold atomic distances. These values (and similarly the lattice parameters *a* and *b*) are subject to further variations (up to about $\pm$ 0.3 Å) due to the periodic oscillations of the contracted interatomic distance around its mean value. The experimental verification of these substantial variations is hard to achieve on the molecular scale as they occur locally (changing from one molecule to its neighbor) and hardly can be measured. Only the mean global variations from one domain to the other can be clearly determined (Figure 5), as in this case it is possible to average the distances over several molecular strides and hence reduce the error.

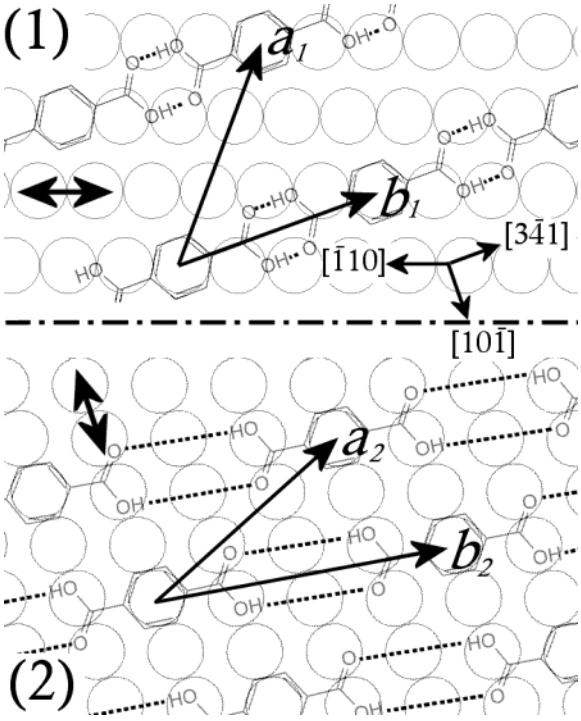

Figure 6. Model showing the effect of the uniaxial contraction of the (22 $\times$ $\sqrt{3}$) reconstruction on the molecular superlattice. Note the differences in the H-bond lengths and in the molecule orientation. Domain types (1) and (2) correspond to those in Table 1 and in the STM image of Figure 5. The substrate atomic distances are greatly exaggerated to emphasize the differences in the molecular lattice. The contraction direction is indicated by a double arrow ([1$\bar{1}$0] in domain (1), [$\bar{1}$01] in domain (2)). The complex structure of the substrate domain boundary is not represented.

The presented values are calculated on the basis of the projected molecular length of 7.02 Å (distance between the two extreme oxygen atoms, cf. Figure 1) in the bulk phase.[22] For an adsorbed geometry, the molecule is probably slightly distorted and the covalent bonds elongated.[32,33] As a comparison, the stretching is ~0.2 Å for PEBA on Ag(111), a 13 Å long organic molecule containing two aromatic rings.[34] Furthermore, the relaxation and therefore the equilibrium shape of the molecules within the superlattice may differ when the intermolecular distances are changed. Both effects can lead to modulations of the hydrogen bond length and induce a correction, which is however expected to be small.

To examine the molecular distortions in more detail, we performed DFT calculations on a free one-dimensional molecular chain. The system is taken as a free chain because the interaction of benzene-derived (π-bonded) molecules with noble metal surfaces is weak and poorly described by the present exchange correlation functionals in the Kohn−Sham method.[35] Also since the adsorption on Au(111) proved to be especially weak, the effect of the substrate on the molecules is small. We performed the DFT calculations within a plane wave basis set up to the cutoff energy of 29Ry, and held the TPA molecule in a super-cell geometry.[36] The Perdew-Burke-Ernzerhof exchange correlation functional,[37] relying on a generalized gradient approximation (GGA), was employed in the Kohn−Sham equations. The lattice constant along the molecular axis and thereby the distance between the neighboring molecules was varied, and the cell dimensions perpendicular to this axis were kept at 10 Å due to the weak interaction. Two *k* points were used along the reciprocal lattice vector corresponding to the molecular axis, and convergence was tested by doubling the

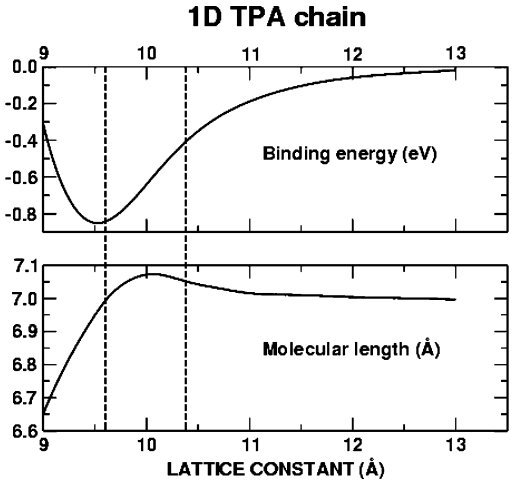

Figure 7. DFT calculations on free 1D molecular chains illustrating the variations in the intermolecular binding energy (upper part) and in the molecular length (lower part) when varying the intermolecular distance. The dashed lines delimitate the lattice parameter range found in Table 1. The results indicate minor variations in the molecular lengths. The variations in the binding energy (calculated per molecule) is only indicative, as the interaction with the substrate is not included in the calculations.

number of *k* points at small lattice constants, where the interaction and thus dispersion is at its largest; this led to practically identical results with the smaller *k* point set, demonstrating an excellent convergence in the Brillouin zone summation.

The DFT results are shown in Figure 7. The maximum elongation calculated for the different domain configurations is of the order of +0.1 Å, whereby the main response pertains to the C−C bond between the carboxylic acid group and the aromatic ring. This value is fairly less than the variations reported in Table 1. Furthermore, it appears that the H-bond lengths found are appreciably larger than in the TPA bulk phase. This difference suggests a moderate to weak character of the H bridge in the adsorbed phase.[38,39,40] These findings are in agreement with the trend emerging for hydrogen-bonded systems at surfaces, where typically increased H-bond lengths occur.[9,11,34]

Variations in the H-bonding lengths are similarly encountered in the relaxation of TPA sheets at intralayer defects. As an example, Figure 8 shows such a long-range relaxation of the molecular film in the vicinity of an edge dislocation. Note that the dislocation does not induce any change in the molecular organization of the surrounding area which consists of a single domain.

We could find no evidence in the STM data for a favored orientational domain as one could expect from the different hydrogen bonding characteristics. To find the domain of lowest energy, we annealed the sample up to 350 K, but we could observe no apparent change in the layer. It is very difficult to gather correct statistics on the basis of the STM images because on the one hand a reconstruction domain can include several nonequivalent TPA domains and on the other hand a TPA domain can cover several reconstruction domains. In this case the complex structure of the substrate reconstruction domain boundary induces local distortions in the molecular superstructure which probably account for a soft transition from one domain type to the other. Nevertheless, there is a correlation between reconstruction and molecular domain boundary as shown in Figure 9. The molecular domain boundary usually follows the underlying reconstruction boundary. The reason for a change in the molecular orientation from one domain to the other is not clear and is not directly related to an optimization of the H-bond length, as every combination between the three possible types occur.

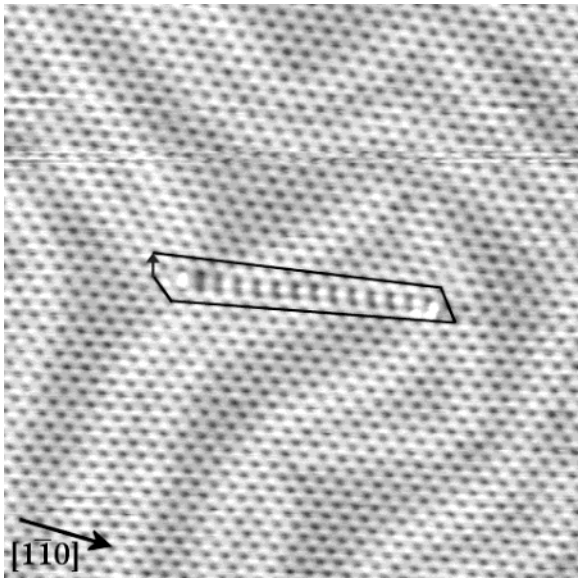

Figure 8. Edge dislocation in the molecular film; the Burger's vector is indicated. The contrast is reversed and the molecules are imaged as depressions (STM image size 27 × 27 nm^2, I = 1.0 nA, V = −360 mV).

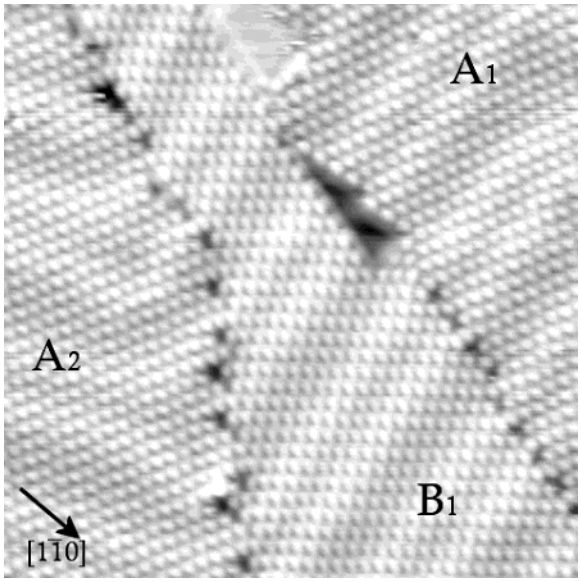

Figure 9. STM image illustrating the correlation between the Au(111) reconstruction domains and the molecular domain boundary. Different domains are labeled. The letter refers to the absolute orientation, the numerical index refers to the domain type detailed in Table 1, i.e., the orientation relative to the underlying reconstruction domain (image size 29 × 29 nm^2, I = 0.5 nA, V = −180 mV).

Conclusion

In conclusion, the self-assembly of terephthalic acid molecules on the Au(111) surface has been investigated by STM at room temperature. At high coverage, the molecules form a highly ordered dense layer. Six domain orientations are observed resulting from the 3-fold rotational substrate symmetry and the 2D chirality of the supramolecular lattice. The dominating intermolecular interaction is head-to-tail coupling by formation of hydrogen bonds. The length of the H-bridges exceeds that in the TPA bulk phase. We modeled the molecular superstruc-

ture and found that the varying periodicity of the uniaxially contracted Au surface induces substantial modulations in the hydrogen bond length of up to 20%. These modulations induce a minor response in the shape of the molecule. DFT calculations indicate a corresponding molecular elongation of max. 0.1 Å.

Acknowledgment. Financial support from the Swiss National Science Foundation is gratefully acknowledged.

References and Notes

(1) Atwood, J. L., Davies, J. E. D., MacNicol, D. D., Vögtle, F., Lehn, J.-M., Eds.; *Comprehensive Supramolecular Chemistry*; Pergamon: New York, 1996.

(2) Reinhoudt, D. N., Ed. *Supramolecular materials and technologies*; Wiley: Chichester, U.K., 1999.

(3) Barth, J. V.; Weckesser, J.; Cai, C.; Günter, P.; Bürgi, L.; Jeandupeux, O.; Kern, K. *Angew. Chem., Int. Ed*. **2000**, *39*, 1230−1234.

(4) Yokoyama, T.; Yokoyama, S.; Kamikado, T.; Okuno, Y.; Mashiko, S. *Nature* **2001**, *413*, 619−621.

(5) Barth, J. V.; Weckesser, J.; Trimarchi, G.; Vladimirova, M.; Vita, A. D.; Cai, C.; Brune, H.; Günter, P.; Kern, K. *J. Am. Chem. Soc*. **2002**, *124*, 7991−8000.

(6) Lin, N.; Dmitriev, A.; Weckesser, J.; Barth, J. V.; Kern, K. *Angew. Chem., Int. Ed*. **2002**, *41*, 4779.

(7) Dmitriev, A.; Lin, N.; Weckesser, J.; Barth, J. V.; Kern, K. *J. Phys. Chem. B* **2002**, *106*, 6907−6912.

(8) Barth, J. V.; Weckesser, J.; Lin, N.; Dmitriev, A.; Kern, K. *Appl. Phys. A* **2003**, *76*, 645.

(9) Feyter, S. D.; Schryver, F. C. D. *Chem. Soc. Rev*. **2003**, *32*, 139−150.

(10) Dmitriev, A.; Spillmann, H.; Lin, N.; Barth, J. V.; Kern, K. *Angew. Chem., Int. Ed*. **2003**, *42*, 2670−2673.

(11) Spillmann, H.; Dmitriev, A.; Lin, N.; Messina, P.; Barth, J. V.; Kern, K. *J. Am. Chem. Soc*. **2003**, *125*, 10725−10728.

(12) Theobald, J. A.; Oxtoby, N. S.; Phillips, M. A.; Champness, N. R.; Beton, P. H. *Nature* **2003**, *424*, 1029−1031.

(13) Krische, M. J.; Lehn, J.-M. *Struct. Bond*. **2000**, *96*, 3−29.

(14) Prins, L. J.; Reinhoudt, D. N.; Timmerman, P. *Angew. Chem., Int. Ed*. **2001**, *40*, 2382.

(15) Böhringer, M.; Morgenstern, K.; Schneider, W.-D.; Berndt, R.; Mauri, F.; Vita, A. D.; Car, R. *Phys. Rev. Lett*. **1999**, *83*, 324−327.

(16) Griessl, S.; Lackinger, M.; Edelwirth, M.; Hietschold, M.; Heckl, W. M. *Single Mol*. **2002**, *3*, 25−31.

(17) Desiraju, G. R. *Crystal engineering: The design of organic solids*; Elsevier: Amsterdam, 1989.

(18) Yaghi, O. M.; O'Keeffe, M.; Ockwing, N. W.; Chae, H. K.; Eddaoudi, M.; Kim, J. *Nature* **2003**, *423*, 705−714.

(19) Lingenfelder, M. A.; Spillmann, H.; Dmitriev, A.; Stepanov, S.; Lin, N.; Barth, J. V.; Kern, K. *Chem. Eur. J*. **2004**, *10*, 1913.

(20) Kim, Y.-G.; Yau S.-L.; Itaya K. *Langmuir* **1999**, *15*, 7810.

(21) Bailey, B.; Crown, C. J. *Acta Crystallogr*. **1967**, *22*, 387.

(22) Sledz, M.; Janczak, J.; Kubiak, R. *J. Mol. Struct*. **2001**, *595*, 77−82.

(23) Parker, B.; Immaraporn, B.; Gellman, A. J. *Langmuir* **2001**, *17*, 6638−6646.

(24) Barth, J. V.; Brune, H.; Behm, R. J.; Ertl, G. *Phys. Rev. B* **1990**, *42*, 9307−9318.

(25) Weckesser, J.; Vita, A. D.; Barth, J. V.; Cai, C.; Kern, K. *Phys. Rev. Lett*. **2001**, *87*, 096101.

(26) Clair, S. Ph.D. Thesis, Ecole Polytechnique Fédérale de Lausanne, Switzerland, 2004.

(27) Sandy, A. R.; Mochrie, S. G. J.; Zehner, D. M.; Huang, K. G.; Doon Gibbs *Phys. Rev. B* **1991**, *43*, 4667.

(28) Narasimhan, S.; Vanderbilt, D. *Phys. Rev. L*. **1992**, *69*, 1564.

(29) Barth, J. V.; Behm, R. J.; Ertl, G. *Surf. Sci*. **1995**, *341*, 62.

(30) Sautet, P. *Chem. Rev*. **1997**, *97*, 1097.

(31) Friebel, D.; Mangen, T.; Obliers, B.; Schlaup, C.; Broekmann, P.; Wandelt, K. *Langmuir* **2004**, *20*, 2803.

(32) Meyerheim, H. L.; Gloege, Th. *Chem. Phys. Lett* **2000**, *326*, 45.

(33) Meyerheim H. L.; Gloege, Th.; Sokolowski, M.; Umbach, E.; Bäuerle, P. *Europhys. Lett*. **2000**, *52* (2), 144.

(34) Vladimirova, M.; Trimarchi, G.; Baldereschi, A.; Weckesser, J.; Kern, K.; Barth, J. V.; De Vita, A. *Acta Mater*. **2004**, *52*, 1589.

(35) Seitsonen, A. P. unpublished results; De Vita, A. private communication.

(36) Specifically, we used the Vienna ab initio simulation package [Kresse, G.; Furthmüller, J. *Phys. Rev. B* **1996**, *54* 11169] and described the electron−ion interaction using the projector augmented wave method [Blöchl, P. E. *Phys. Rev. B* **1994**, *50*, 17953−17979. Kresse, G.; Joubert, D. *Phys. Rev. B* **1999**, *59*, 1758].

(37) Perdew, J. P.; Burke, K.; Ernzerhof, M. *Phys. Rev. Lett*. **1996**, *77*, 3865; Erratum **1997**, *78*, 1396.

(38) Steiner, T. *Angew. Chem., Int. Ed*. **2002**, *41*, 48−76.

(39) Desiraju, G. R. *Acc. Chem. Res*. **2002**, *35*, 565−573.

(40) Desiraju, G. R.; Steiner, T. *The Weak Hydrogen Bond*; Oxford University Press: Oxford, U.K., 1999.

(41) Barth, J. V.; Behm, R. J.; Ertl, G. *Surf. Sci. Lett*. **1994**, *302*, L319.